Soft Matter

PAPER

View Article Online
View Journal | View Issue

Cite this: *Soft Matter*, 2025, **21**, 6919

Phase behavior of catenated-linear DNA mixtures

Indresh Yadav [ab] and Patrick S. Doyle *[a]

Received 6th May 2025,
Accepted 8th August 2025

DOI: 10.1039/d5sm00461f

rsc.li/soft-matter-journal

Understanding the phase behavior of multicomponent systems is crucial in condensed matter physics, both for practical applications and fundamental exploration. Regardless of chemical composition, topology stands out as a crucial parameter in this context. We studied herein the phase behavior of a 2D catenated network of DNA rings called a kinetoplast in the presence of linear DNA. We examine the system at a fixed kinetoplast DNA concentration and linear DNA size, while varying the concentration of linear DNA. The mixing of circular DNA with linear DNA is reported to lead to the isotropic phase of the mixtures, however, catenated DNA rings (the assembly of circular DNA) lead to the phase separation in the presence of linear DNA. This distinction highlights the profound influence of topology on the phase behavior of polymer blends. The phase-separated aggregates of kinetoplasts exhibit a fractal nature, with the fractal dimension indicating the dominance of the diffusion-limited mechanism in the aggregation process. Although the structure of these aggregates is robust, significant thermal fluctuations in size and shape occur at various length scales. The understanding of the bulk phase behavior of the catenated DNA network provides crucial insights in designing the catenated-linear polymer composites.

1. Introduction

The study of phase behavior of multicomponent systems is of fundamental interest across condensed matter physics, finding practical applications in diverse domains like medicine, food industry, and metallurgy.[1–5] Polymeric mixtures, comprising blends, block copolymers, and polymer solutions, present a captivating arena to study phase transitions and self-assembly.[6–9] Diverse molecular architectures, chain conformations, and intermolecular forces dictate the equilibrium microstructures of the polymeric systems, which can further be tuned by solvent quality (*e.g.*, ionic strength and pH), temperature, and confinement.[10–12] Notably, intricate interactions between protein chains have been observed to drive liquid–liquid phase separation and are believed to be responsible for membranelles organelles within eukaryotic cells.[13,14] Intracellular phase separation also has implications in neurodegenerative diseases like amyotrophic lateral sclerosis (ALS), Alzheimer's, and Huntington's disease, where solid-like protein inclusions composed of semi-crystalline amyloid fibers.[15] Exploring polymeric assembly not only provides a robust framework to uncover the fundamental principles governing biological assembly at the cellular level but also provides an avenue for novel soft materials.[16–18]

In pursuit of understanding the biological function of biomolecules, as well as creating new synthetic materials, DNA with varying architectures has been widely studied.[19–24] For instance, entangled mixtures of ring and linear DNA have been shown to exhibit enhanced shear thinning and viscosity, as well as prolonged relaxation timescales, surpassing those observed in pure solutions of either rings or linear chains.[23–25] These emergent features stem from the synergistic interweaving of rings by linear DNA. While linear polymers induce demixing and semi-crystalline phases at higher concentrations, interestingly, the mixture of linear and circular polymers always remains in isotropic phase with enhanced miscibility.[26–28] Thus, despite having the same chemical compositions, the statistical properties are significantly influenced by the topological states of a polymer,[29] which have a profound impact on the phase behavior and rheological properties of polymeric blends.[23,30]

Given the prominent role of topology, linear polymers and their derivatives (*e.g.*, rings, stars, ladders, knots, and 3D networks) have been extensively investigated.[31,32] In a similar line polymers with mechanical bonds (*e.g.*, rotaxane and catenane) have been a topic of current studies.[33] Particularly catenanes can exist with global topology of 1D, 2D, or 3D, along with varying degrees of catenation in 2D and 3D. One such system is found in nature in the form of kinetoplast DNA (kDNA). kDNA from trypanosomatid *Crithidia fasciculata* is a natural *Olympic gel* wherein approximately 5000 minicircles (~2.5 kbp, contour length 850 nm) and 25 maxicircles (~40 kbp, contour length

[a] *Department of Chemical Engineering, Massachusetts Institute of Technology, Cambridge, Massachusetts 02139, USA. E-mail: pdoyle@mit.edu*
[b] *Department of Physics, Indian Institute of Technology Bhubaneswar, Odisha 752050, India*

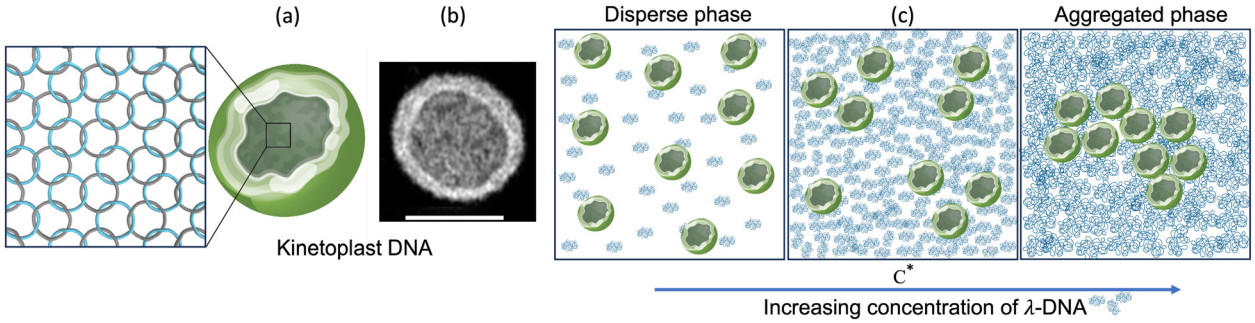

Fig. 1 Model schematic of the molecular topology of kinetoplasts and its transition from disperse phase to aggregate phase. (a) Schematic diagram of a kinetoplast, a catenated 2D network (Olympic gel) made of thousands of interlocked rings of circular DNA. The average catenation valency of minicircles is 3. (b) Super-resolution confocal microscopy image presenting the kinetoplast shape *in vitro* under good solvent condition, which can be described as a wrinkled bowl with positive Gaussian curvature. (c) Schematic diagram representing the phase evolution of kinetoplast in the presence of λ-DNA. Here λ-DNA is depicted in coil form and C^* represents the overlap concentration (42 μg mL^{-1}) of λ-DNA. Scale bar in (b) is 5 μm.

13.6 μm) are topologically interlocked in a quasi-2D plane.[34] A simplified structure of a kDNA molecule along with a super-resolution confocal microscopy *in vitro* is presented in Fig. 1(a and b). The extension of a kDNA molecule in 2D plane is approximately 5 μm. The catenation valency of minicircles is approximately 3,[34–37] however, the catenation valency of maxicircles is unknown. While the network of maxicircles and minicircles are interlocked with each other, each network can be sustained independently.[38]

Recently, kDNA has been extensively studied, particularly at the single molecule level.[39–46] It not only attracts as a model for catenated polymer and Olympic gels, but it also presents a unique model system for 2D polymers owing to its global topology. For example, it has been shown that in response to constriction or electric field stretching, kDNA behaves as an elastic sheet.[39,40] Its properties as a 2D polyelectrolyte have also been studied in response to the degree of confinement, ionic strength, and crowding.[41–43] Moreover, we recently introduced a novel approach to selectively manipulate the physical characteristics of kDNA using restriction enzymes.[44] Heterogeneity in the base-pair sequencing of different classes of rings has been used to selectively cut and remove a fraction of rings from the network, and hence tune the topology. Remarkably, regardless of the intricacies of molecular topology, we discovered a universal scaling relationship between the time constant of shape fluctuations and the variance of shape anisotropy. Recent studies using high-resolution AFM imaging probed deeper into the intrinsic topological and geometrical features of kDNA molecules.[46–49] Despite significant progress in single-molecule studies of kDNA, there is no study on its bulk phase behavior or rheological properties.

Herein we study the phase behavior of kDNA in the presence of linear DNA. The concentration of kDNA has been kept fixed (25 μg mL^{-1}) while its evolution has been observed as a function of the concentration of linear λ-DNA. λ-DNA consists of 48 502 base pairs and has a contour length of 16.5 μm. In a good solvent and dilute solution, its radius of gyration is approximately 0.7 μm,[50] making its spatial extension approximately seven times smaller than that of a kDNA molecule. A schematic representing the typical phase behavior of the kinetoplasts in the presence of λ-DNA in different regimes is presented in Fig. 1(c). In the dilute regime of λ-DNA concentration (below the overlap concentration C^*), kDNA remains in the dispersed phase hence forming a stable equilibrium blend. Increasing the concentration of λ-DNA above C^* leads to the aggregation of the kDNA. Here, C^* represents the overlap concentration of pure linear λ-DNA, which is about 42 μg mL^{-1}.[51] This result is completely distinct from the phase behavior observed for the dispersion of circular DNA in the presence of linear DNA, where enhanced mixing is well established.[26,27] This distinction highlights the profound influence of topology on the phase behavior of polymer blends. Our findings reveal that the aggregates formed by kinetoplasts exhibit fractal characteristics, indicating a diffusion-limited mechanism in their formation. Although these aggregates maintain a stable structure, thermal fluctuations cause variations in size and shape across different length scales. The understanding of the bulk phase behavior of catenated DNA networks provides crucial insights into designing catenated-linear polymer composites.

2. Materials and methods

2.1. Sample preparation

Kinetoplasts (kDNA) from trypanosomatid *Crithidia fasciculata* were purchased from TopoGEN Inc. Received kDNA solution has a concentration of 612 mg mL^{-1}. The solvent was TE buffer, which is composed of 10 mM Tris-HCl, pH7.5, and 1 mM EDTA. Bacteriophage λ-DNA (48.5 kbp, contour length of 16.5 μm) was purchased from New England Biolabs, Ipswich, MA. As received from the manufacturer the λ-DNA stock solution has a concentration of 500 mg mL^{-1}. The solvent was TE buffer, which is composed of 10 mM Tris-HCl, pH 8.0, and 1 mM EDTA. To remove naturally formed concatemers of λ-DNA, the stock solution was heated to 65 °C for 10 min, then rapidly cooled to 23 °C by immersion in a water bath. To have a stronger binding of the dye molecules to kDNA and overcome the

influence of ionic strength on the dye-DNA interaction kinetics, we used MFP488 MIRUS dye which binds covalently to nucleotides.[52] The staining ratio of the dye molecule to the DNA base pair was about 1 : 160. The reaction protocol was adopted as suggested by the manufacturer, however, a purification protocol was developed. After the binding reaction was completed, the sample was centrifuged in 100 kDa cut-off membrane (Amicon Ultra Centrifugal Filter, Merck) at room temperature at 5000 *g* for 5 times and each run for 2 minutes to remove the unbound dye and redisperse the sample in 0.5× TBE buffer (pH 8). Glass coverslips were cleaned with ethanol and soaked at least 1 hour in 1 M NaOH. Samples were imaged inside the microwell created on microscope coverslip using Frame Seal Slide Chambers purchased from Bio-Rad Laboratories.

2.2. Fluorescence imaging

The solution containing the stained kinetoplast (kDNA) molecules was mixed with unstained λ-DNA in 0.5× TBE buffer in addition to 25 mM NaCl. Samples were gently mixed with wide-cut tips and 25 μL samples were deposited in the well created using a Frame Seal chamber. To understand the phase behavior of kDNA in the presence of λ-DNA we used a super-resolution laser scanning confocal microscope. A Zeiss LSM 980 with Airyscan 2 microscope was used in oil-immersion mode with a 63× objective (numerical aperture 1.4). For each sample, a 25 μL volume was placed inside a well measuring 9 mm × 9 mm in length and width, with a depth of 310 μm. Images were captured at the bottom of the chamber, just above the coverslip. Images were analyzed using ImageJ and home-built scripts in MATLAB (MathWorks, Natick, MA).

3. Results and discussion

Electromagnetic interaction, in the form of screened-Coulomb interaction, hydrogen bonds, and van der Waals interaction, along with entropy due to thermal energy decide the self-assembly and phase behavior of the polymeric system.[11] Variations in the size and flexibility of molecules within a blend of two polymer species can lead to entropy-driven depletion attraction, where one type of molecule experiences attraction in the presence of the other.[7,53] We can systematically tune the balance between these forces. For instance, by screening electrostatic repulsion, it becomes possible for different segments of the polymeric chain or distinct polymeric molecules to approach closely enough. This proximity enables attractive interactions (*e.g.*, van der Waals, bridging, depletion) to dominate. In this contribution, we studied the phase behavior of kDNA in the presence of linear λ-DNA. The system is investigated in tris-boric acid-ethylenediaminetetraacetic acid (0.5× TBE, pH 8) buffer with an ionic strength of 32.3 mM.[41] The zeta potential of kDNA dispersed in this buffer was measured to be −70 ± 4 mV. To screen the Coulombic repulsions between the DNA chains, an additional 25 mM of NaCl is added. Thus the resultant ionic strength of the solution is 57.3 mM corresponding to a Debye length of 1.27 nm compared to the 2 nm bare width of dsDNA.

Although the concept of overlap concentration is well established for linear polymers, its definition is less straightforward for complex topologies like kDNA. Single-molecule studies suggest that kDNA can be treated as a soft colloidal particle with an asymmetric shape and multiple possible orientations.[39,40,43] At sufficiently high concentrations, such particles begin to interact *via* excluded volume effects. We refer to the corresponding concentration as the overlap concentration for kDNA. To estimate this C^*_{kDNA}, we approximate each kDNA as a disk of diameter D = 5 μm and thickness t = 2.5 μm.[39,44] At the experimental ionic strength of 57.3 mM, the Debye length is approximately 1.27 nm. Thus, the range of screened Coulomb interactions is negligible compared to the physical dimensions of kDNA. Orientationally averaged excluded volume for monodisperse disks has been calculated by Onsager to be $V_{\mathrm{ex}} \approx \frac{\pi}{4}\left(\frac{D}{t}\right) V_{\mathrm{p}}$, where $V_{\mathrm{p}} = \frac{\pi}{4} D^2 t$ is the volume of a disk.[54] Inputting values for kDNA results in $V_{\mathrm{ex}} \approx 77.1\ \mu\mathrm{m}^3$. Including the contribution of 5000 minicircles (each 2.5 Kbp) and 25 maxicircles (each 40 Kbp) a single kDNA molecule contains 13.5 Mbp. Using the mass of 1 bp as 650 Dalton, the molecular mass of a kDNA molecule is $M = 8.78 \times 10^9\ \mathrm{g\ mol^{-1}}$. The mass of a single kDNA molecule is therefore $m = M/N_{\mathrm{A}} \approx 1.46 \times 10^{-14}$ g, where N_{A} is Avogadro's number. The estimated overlap concentration is then $C^*_{\mathrm{kDNA}} = m/V_{\mathrm{ex}} \approx 190\ \mu\mathrm{g\ mL^{-1}}$. The concentration of kDNA used in our experiments is 25 μg mL^{-1}, which is approximately seven times lower than the overlap concentration, indicating that the kDNA solution can be considered well within the dilute regime. Despite being in the dilute regime, the presence of kDNA molecules influences the configurational crowding experienced by λ-DNA and alters its effective overlap concentration (see SI for an estimation of this effect). Nevertheless, in our analysis, we have treated C^* as if it were defined for pure λ-DNA, without accounting for the additional crowding introduced by kDNA.

Fig. 2 presents snapshots of kDNA, imaged using a super-resolution confocal microscope. The concentration of kDNA is kept fixed (25 μg mL^{-1}), however, the concentrations of λ-DNA are varied in the range (0–150 μg mL^{-1}, *i.e.*, 0–3.6C^*). Here, C^* represents the overlap concentration of pure linear λ-DNA. Moreover, only kDNA molecules have been labeled with fluorescent dye *i.e.*, λ-DNAs are invisible. It is evident that in the absence of λ-DNA, kDNA molecules are well dispersed in the solution and present an isotropic and homogeneous solution (Fig. 2(a)). As we add a small fraction (0.3C^* and 0.6C^*) of λ-DNA, (Fig. 2(b and c)), the isotropy and homogeneity of the solution are quite similar to the bare kDNA sample, and no sign of aggregation and evolution of system over time has been observed (Fig. S1). However, with further increasing λ-DNA concentration the system shows the tendency to aggregate which finally leads to the aggregation of kDNA. The nature of the aggregates varies with the concentration of λ-DNA. For example, at 1.2C^* (Fig. 2(d)), the clusters lack well defined size and shape. The clusters are highly dynamic, with diffuse

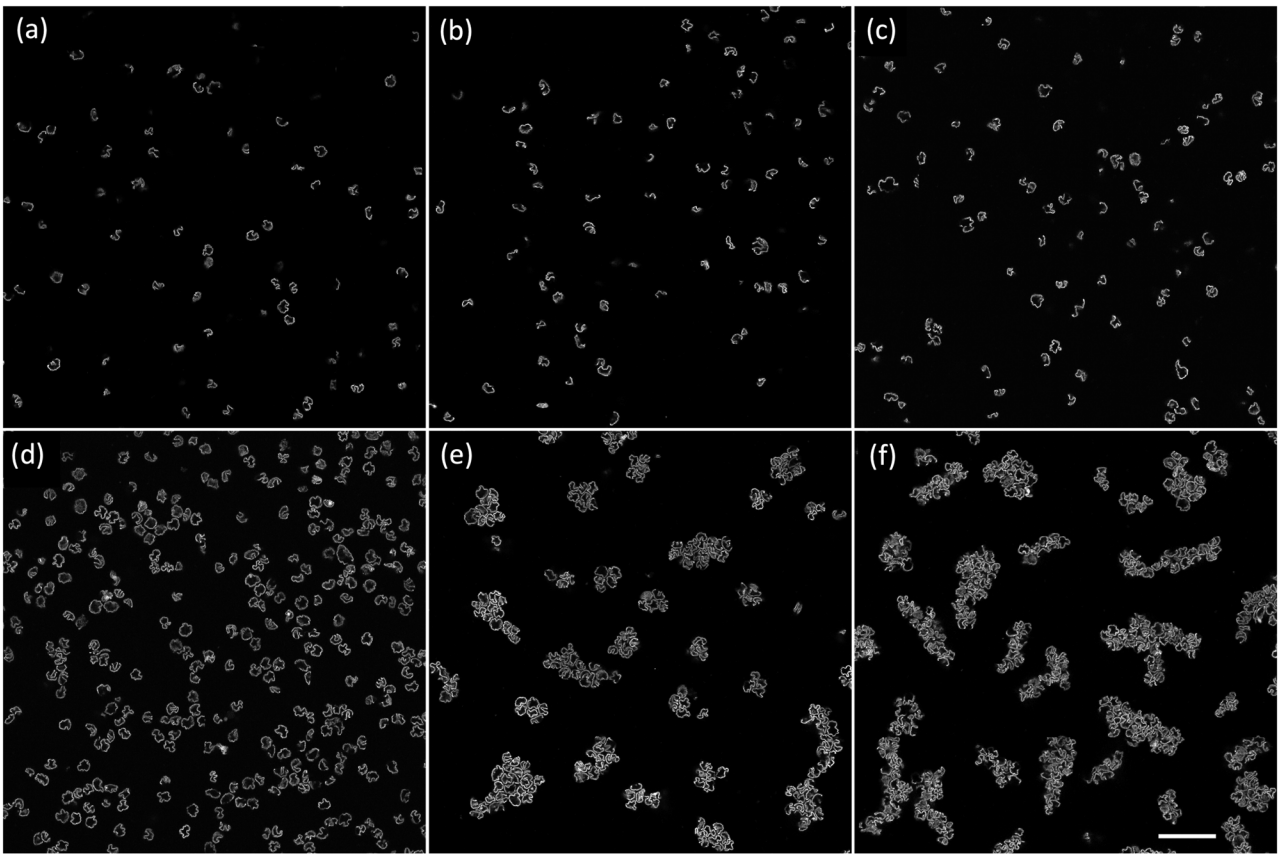

Fig. 2 Confocal microscopy images showing the phase behaviour of kDNA (25 μg mL^{-1}) at varying concentrations of λ-DNA. Image (a) shows the control with no λ-DNA. Images (b) to (f) show kDNA solutions with increasing concentrations of λ-DNA: 12.5 μg mL^{-1} (0.3C*), 25 μg mL^{-1} (0.6C*), 50 μg mL^{-1} (1.2C*), 100 μg mL^{-1} (2.4C*), and 150 μg mL^{-1} (3.6C*). The phase solution of kDNA evolves over time depending on the λ-DNA concentration. No further evolution was observed at 2.4C* after 5 hours, indicating that the kDNA–λ-DNA mixture had reached a steady state. Observation times for other λ-DNA concentrations were adjusted using a scaling relation ($\eta \sim C$), which reflects how solution viscosity (η) affects the diffusion timescale of individual kDNA molecules. The images shown correspond to the respective observation times for 0.3C*, 0.6C*, 1.2C*, and 3.6C*, which are 37.5 minutes, 1 hour 15 minutes, 2 hours 30 minutes, and 7 hours 30 minutes, respectively. Scale bar is 20 μm.

boundaries and noticeable exchange of kDNA molecules with both the surrounding medium and neighboring clusters. This exchange behavior appears to be governed more by λ-DNA concentration than by the size of the kDNA clusters. Despite this activity, the overall system remains stable over time, with no evidence of cluster growth or large-scale phase separation (Fig. S1). However, at 2.4C* and 3.6C* the size and shape of kDNA aggregates are well-defined, where individual kDNA molecules are tightly held in aggregates (Fig. 2(e and f)). Though there is significant conformational fluctuation in individual molecules in aggregates (see Movie SM1), kDNA molecules are not exchanged from aggregates to solution.

The dispersion of kDNA in the presence of λ-DNA exhibits a *meta*-stable state with continuous evolution, selecting an appropriate time point for comparing systems with different λ-DNA concentrations presents an experimental challenge. To address this, we first identified the optimal imaging time for systems containing 2.4C* of λ-DNA. This time was identified as approximately 5 hours after sample preparation, when the size of individual kDNA aggregates showed no significant change, indicating a quasi-equilibrium state. Based on the premise that the behavior of aggregates is primarily governed by the diffusion of individual kDNA molecules, a hypothesis supported by subsequent discussions on aggregate characteristics, we extrapolated the characteristic diffusion time of kDNA relative to varying concentrations of λ-DNA. Taking the size of the individual kDNA molecules constant regardless of λ-DNA concentration, and using the scaling ($\Delta\eta \sim C^1$) of the solution's viscosity ($\Delta\eta$) in the semi-dilute regime with varying concentration (C) of λ-DNA, we calculated the characteristic diffusion time (τ_b) of kDNA to diffuse a distance equal to its own size. Using the Stokes–Einstein relation and the viscosity scaling, we find $\tau_b \sim C$. To ensure a fair comparison across different concentrations, the experimental time (t) should be adjusted so that t/τ_b remains constant. Thus, the corresponding times for 12.5 μg mL^{-1} (0.3C*), 25 μg mL^{-1} (0.6C*), 50 μg mL^{-1} (1.2C*), and 150 μg mL^{-1} (3.6C*) of λ-DNA are 37.5 min, 1 hour 15 min, 2 hour 30 min and 7 hours 30 min, respectively. Therefore, the images presented in Fig. 2 for different concentrations of λ-DNA were recorded at these respective times. This choice of experimental timing is further validated by the data presented in the comparison of the time evolution of the

system near C^* (Fig. S1), which shows no significant changes over time.

Notably, the viscosity of λ-DNA solutions changes significantly as the concentration approaches the entanglement threshold where individual DNA strands begin to interpenetrate and form an entangled network. This threshold has been reported at different values across studies, depending on the experimental technique employed.[51] Microrheology measurements[55,56] suggest that entanglement occurs around 200 μg mL^{-1}, and in this regime, the viscosity increases sharply, following a scaling law of $\Delta\eta \sim C^{3.93}$.[55] As a consequence, the time required for the system to reach equilibrium decreases at concentrations below $2.4C^*$, but increases substantially above this concentration (see SI). This scaling behavior imposes a temporal boundary. In our experiments kDNA-λ-DNA mixtures equilibrate within the shortest timescale permitted by these scaling laws and remains stable till and beyond the longest timescale at a given λ-DNA concentration. These observations support the conclusion that the systems presented in Fig. 2 have indeed reached equilibrium, as no further structural evolution was observed over time.

Upon learning the critical role of the concentration of λ-DNA in influencing the phase behavior of kDNA, we examined the temporal evolution of the kDNA solution at a fixed concentration of λ-DNA of $2.4C^*$. The evolution is presented in Fig. S1. Initially, the system remains in a dispersed state. However, the introduction of λ-DNA destabilizes the solution, triggering the gradual aggregation of kDNA. With time, these aggregates increase in size. The image montage clearly demonstrates that the individual aggregate grows progressively before reaching a steady state. This growth behavior is further highlighted in the cropped images of Fig. 3(b), extracted from Fig. S2. kDNA initially forms dimers, trimers, tetramers, and larger aggregates, eventually reaching a quasi-equilibrium size. Beyond this point, the aggregates become large enough that their diffusion slows markedly, effectively stopping further growth.

Given an aggregation process governed by diffusive, the relation between the radius of gyration and time can be expressed as $R_g \sim t^{\beta}$, where R_g is the radius of gyration of the aggregate, t evolution time, and β is growth exponent.[57] This feature is captured in Fig. 3(a). The exponent of the evolution of cluster size as a function of time for kDNA in the presence of $2.4C^*$ of λ-DNA is found to be 0.22 ± 0.04 (SD) (SD: standard deviation). Similar values for colloidal aggregates have been reported for different sizes and shapes of hard colloidal particles.[57,58] The value of the growth exponent indeed suggests the dominance of the diffusion-limited mechanism in the aggregation process of kDNA induced by λ-DNA.

To understand the morphological features of kDNA aggregates we calculated the radius of gyration as a function of the number of kDNA molecules in the aggregates. This is presented in Fig. 4. The morphology of aggregates has been extensively studied in various systems.[57–61] Their scale-invariant nature is often characterized by the relationship between the spatial extent, quantified by the radius of gyration (R_g), and the mass of the cluster (M), which follows the scaling law $M \sim R_g^d$,[57] where d is the fractal dimension. Assuming that the mass of the

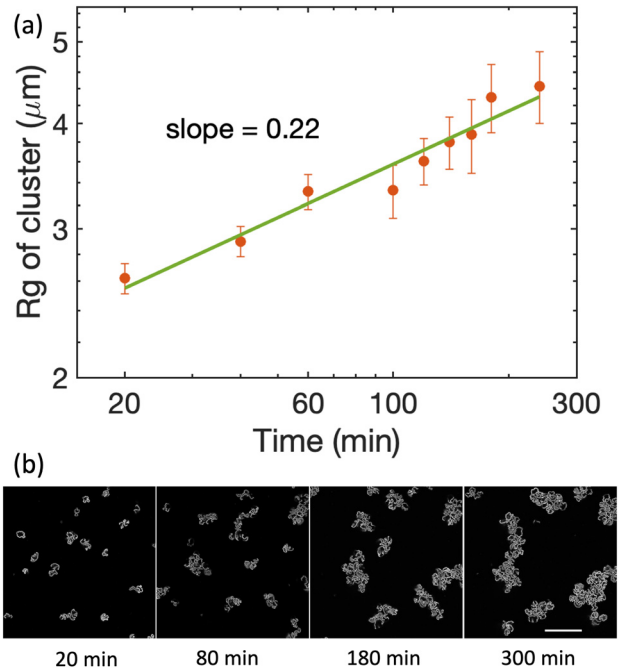

Fig. 3 (a) Scaling relation between the mean cluster size given by radius of gyration and time presents the growth rate of the cluster of kDNA in the presence of $2.4C^*$ of λ-DNA. (b) Sample snapshots presenting the evolution of the kDNA. Scale bar is 20 μm.

cluster (M) is proportional to the number of particles (N)[59] in a cluster, this relation can be rewritten as $R_g \sim N^{\nu}$,[62] where the exponent ν is inversely related to the fractal dimension d, that is, $d = 1/\nu$. The fractal dimension d is a widely adopted metric for assessing aggregate morphology and structure. In the realm of two-dimensional solid objects, a canonical value of d is 2, signifying a non-fractal structure. However, when d falls below 2, it signals a fractal arrangement characterized by a density decrease as the value of d decreases. A value of 2 is anticipated at length scales below the diameter of kDNA. The value of the fractal dimension, d, of kDNA aggregates in the presence of $2.4C^*$, and $3.6C^*$ of λ-DNA are found to be 1.6 ± 0.1 (SD) and 1.5 ± 0.1 (SD), respectively. These two values are statistically not different thereby the degree of packing and qualitative nature of kDNA aggregates are insensitive to the concentration of λ-DNA. However, the average size ($\langle R_g \rangle$) of kDNA aggregates in the case of $3.6C^*$ (7.2 μm) is relatively higher compared to $2.4C^*$ (6.1 μm) (Fig. 2(e and f)).

It should be noted that the value of d is calculated from the 2D planar cross-section of the aggregates, inherently possessing 3D characteristics. This approach is adopted due to an experimental limitation, namely the challenge of counting the number of kDNA molecules within aggregates in a full 3D space. This strategy is widely employed in colloidal science to overcome such experimental constraints.[58,59]

The observed fractal dimension of the kDNA aggregates is relatively low compared to the commonly reported range of 1.70–1.85 for diffusion-limited cluster aggregation (DLCA) in spherical colloids.[58,60,62] However, it is important to note that

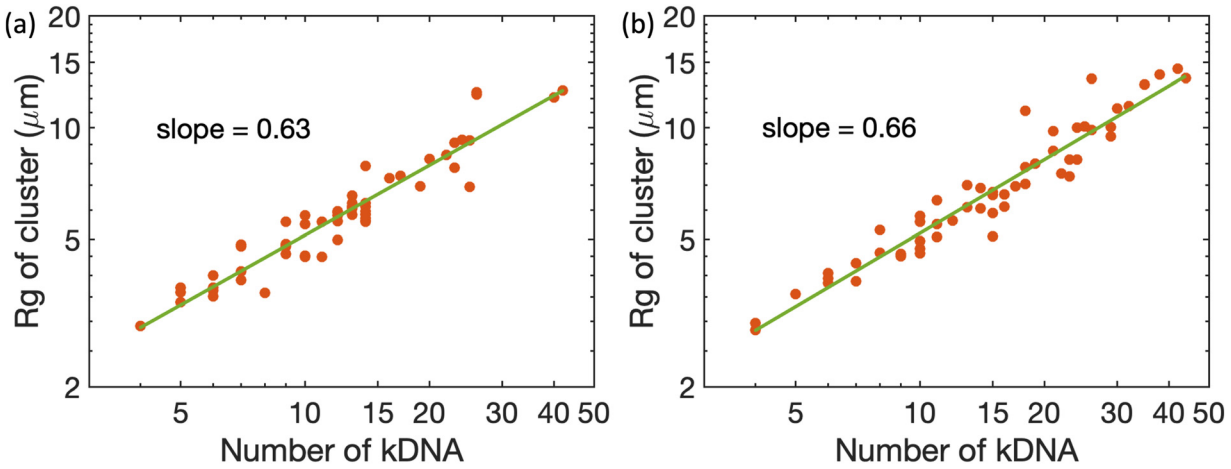

Fig. 4 Scaling relation between the cluster radius of gyration to the number of kDNA in the aggregates for two different concentrations of λ-DNA (a) 2.4C^* and (b) 3.6C^*. From the slope of the linear fit to the data we extract a fractal dimension (1/slope) of 1.6 ± 0.1, and 1.5 ± 0.1 for 2.4C^* and 3.6C^*, respectively.

the fractal dimension is known to be sensitive to both the geometry[61] and the size of the colloidal particles,[58] with d typically decreasing as the particle size increases. Because kDNA molecules are significantly larger than gold, silica, or polystyrene nanoparticles, systems for which the aggregation behavior has been extensively studied, this size dependence is particularly relevant. Based on a *meta* study showing a decrease in fractal dimension with increasing particle size,[58] the measured value for kDNA aggregates (d = 1.6 ± 0.1 (SD)) suggests that its aggregation in the presence of λ-DNA is primarily governed by a diffusion-limited aggregation (DLA) process.

Furthermore, there is no evidence of intramolecular aggregation of kDNA segments even at the maximum concentration of λ-DNA in this study. This feature of the present system is completely different from the conformational phase behavior of dilute kDNA in the presence of poly(ethylene glycol) (PEG) with a molecular weight of 10 kDa,[43] where intramolecular aggregation is prominent at higher concentrations of PEG. In the case of added PEG, kDNA first exhibit local clustering of chain segments displayed as bright foci and then at higher PEG concentration collapse of the kDNA to a compact spheroid. The size (radius of gyration) of the 10 kDa PEG is about 2 nm which is much smaller than the average mesh size (∼34 nm) of the pristine kDNA network.[46] The PEG molecules penetrate the kDNA network and tend to maximize the available volume by pushing the segments of a network together through depletion mechanics.[63] Thus, the intramolecular phase transition from flat phase to globule phase in the presence of PEG was dictated by the interplay of configurational entropy and intramolecular interactions. With increasing concentration, PEG molecules try to occupy the maximum volume within the system and impose an osmotic pressure on the kDNA network due to excluded volume interactions. This pressure overcomes bending rigidity and intramolecular electrostatic repulsions within kDNA, leading to the collapse of the network through sequential hierarchical steps. Similar features have been observed using atomic force microscopy,[64] where intramolecular compaction of kDNA is driven by protein-mediated bridging interaction.

In this study, we identified a crucial factor regarding the size of λ-DNA. With the contour length of 16.5 μm and radius of gyration 700 nm, λ-DNA notably exceeds the intramolecular mesh size as measured using AFM (∼34 nm) of a kDNA network.[46,49] Consequently, the range over which depletion-induced attraction between the network operates extends far beyond the mesh size. The possible length-dependent nature of excluded volume interactions between kDNA and PEG or λ-DNA is illustrated in SI Figure (S4). This difference in length scales implies that the kDNA network does not experience intramolecular attraction which is evident in the unchanged shape of kDNA irrespective of λ-DNA concentration. However, as the concentration increases, λ-DNA molecules strive to maximize the available volume, leading to the entropically driven depletion-induced intermolecular attraction between kDNA molecules. Yet, despite the attractive depletion force, it is important to note that this force could not overcome the electrostatic repulsion between the charged kDNA molecules. To screen the electrostatic interaction, we added 25 mM of NaCl in the solution. This strategic adjustment allows for the dominance of the depletion attraction to induce the aggregation of kDNA networks above a critical λ-DNA concentration. The strength of the depletion attraction between colloidal particles grows linearly with polymer concentration.[65] Although its range is dictated by the size of the polymers, it remains constant irrespective of concentration in the dilute regime (below C^*). However, the range changes above C^*. This is because, due to coil interpenetration, the effective size of the polymer is determined by the concentration-sensitive blob size.[66] With this adjustment, the Asakura–Oosawa depletion model[63] accurately describes the effective potential across a wide range of λ-DNA concentrations, spanning from dilute to semidilute regimes.[67]

In the present study, intrinsic asymmetry in the shape of individual kDNA molecules poses challenges in quantitatively estimating the interaction potential using the current experimental approach. However, qualitative observations of the aggregation behavior provide insight into the strength of

intermolecular kDNA interactions. Below approximately 1.2C^*, the kDNA solution remains predominantly in a dispersed phase. Even when transient aggregation occurs, the resulting clusters lack well defined size and morphology, and dynamic exchange of kDNA molecules between different regions is frequently observed. Such behavior implies that the net attractive kDNA interactions are weaker than thermal energy (k_BT). In contrast, when the λ-DNA concentration reaches 2.4C^* or higher, the system forms temporally stable clusters. Observations of the cluster relaxation behavior show that the kDNA molecules inside each cluster rearrange themselves, but they do not leave the cluster. Thus for this concentration of λ-DNA, we can infer that kDNA interactions are greater than k_BT.

Although the structure of the aggregates is robust, there are significant fluctuations in size and shape due to thermal energy, as observed in Movies SM1 and SM2. These fluctuations for a single cluster in the presence of 2.4C^* of λ-DNA were quantified by measuring the variation in radius of gyration (size) and aspect ratio (shape) over time, as depicted in Fig. 5(a) and (b), respectively. The radius of gyration (R_g) was determined from the square root of the trace of the gyration tensor, calculated from projected fluorescence intensity.[68] The principal eigenvalues of this tensor provided the lengths of the minor and major axes, from which the aspect ratio (the ratio of minor to major axis) was derived. Aspect ratio values close to 1 indicate a circular disk arrangement, while values near 0 indicate a linear arrangement (rod). The thermal fluctuations of both R_g and aspect ratio are stationary but their relative phase varies across clusters and is often out of phase. A detailed discussion of this behavior is presented in Fig. S5. The mode of size and shape relaxation can be better understood from the autocorrelation function presented in Fig. 5(c).

The autocorrelation functions are fitted using the sum of two exponential terms, represented as $C(\tau) = \alpha + \beta\exp(-t/\tau_1) + \gamma\exp(-t/\tau_2)$, where τ_1 and τ_2 represent the characteristic time scales of two distinct relaxation processes, and the coefficients β and γ indicate their respective contributions. The parameter α is the residual correlation at long times, which ideally approaches zero if the system fully relaxes. For the radius of gyration, two relaxation time constants are $\tau_1 = 3.5 \pm 0.1$ s (SD: standard deviation) and $\tau_2 = 29.0 \pm 1.1$ s (SD). The corresponding amplitudes are $\beta = 0.60 \pm 0.01$ (SD) and $\gamma = 0.16 \pm 0.01$ (SD), indicating that the majority of the correlation

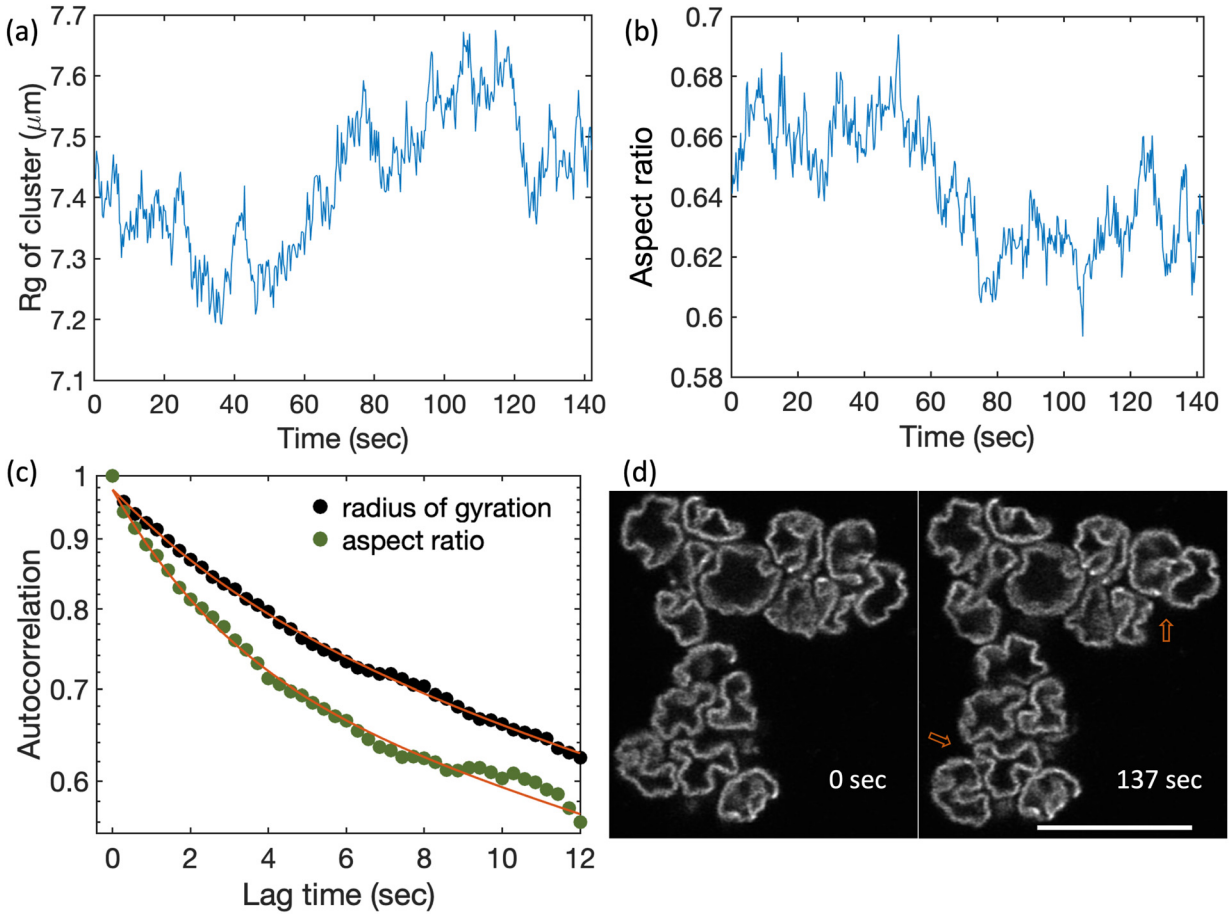

Fig. 5 Temporal behavior of kDNA cluster in the presence of 2.4C^* of λ-DNA. (a) The radius of gyration (R_g) of a representative cluster as a function of time. (b) Aspect ratio (shape anisotropy) of the same cluster as a function of time. (c) Autocorrelation functions of R_g and aspect ratio for the same cluster as in (a) and (b). (d) Snapshots of the same cluster at two different time points. Arrows in (d) highlight the cluster's structural rearrangement. Scale bar in (d) is 20 μm.

decays on the shorter timescale, but a slower component persists, reflecting a delayed relaxation of the cluster size. The residual offset is very small (α = 0.017 $\pm$ 0.002 (SD)), indicating that the size fluctuations fully relax (de-correlate) over the observed time scale. In the case of aspect ratio, the relaxation times are τ_1 = 2.7 $\pm$ 0.1 s (SD) and τ_2 = 50.7 $\pm$ 1.5 s (SD), with corresponding amplitudes β = 0.71 $\pm$ 0.01 (SD) and γ = 0.26 $\pm$ 0.01 (SD). The residual offset is very small (α = 0.012 $\pm$ 0.001 (SD)), indicating that the shape fluctuations fully relax (de-correlate) over the observed time scale.

The presence of two distinct timescales reflects fast local rearrangements and slower, large-scale reorganization within the cluster. Moreover, the fastest mode of aspect ratio relaxes faster than the fastest mode of radius of gyration, further suggesting a hierarchical relaxation process. The internal shape reorganizes more quickly, while the overall size takes longer to reorganise. This behavior is similar with known polymer dynamics, where relaxation can be described by a spectrum of modes.[69,70] Higher order internal modes, related to shape metrics such as asphericity or aspect ratio, relax faster than the lowest order global mode, which governs the relaxation of size related observables (*e.g.* radius of gyration). Simulation studies further support that different geometric parameters of a polymer can relax on distinct timescales.[71] This complexity could not be captured by a single exponential fit, as presented in SI (Fig. S3). One might consider whether the observed relaxation of the clusters arises from the relaxation of the surrounding λ-DNA bath. However, this possibility can be ruled out. Even at the highest λ-DNA concentration used in this study (3.6C^*), the longest relaxation time of λ-DNA remains below 0.5 s,[56] significantly shorter than the smallest relaxation time (2.7 s) observed for the cluster. This confirms that the relaxation dynamics reported here are intrinsic to the kDNA clusters. Notably the relaxation time scale of individual kDNA molecules, in the absence of λ-DNA is much shorter ($\sim$0.2 s)[44] than the smallest relaxation time observed for the cluster. Fig. 5(d) presents the snapshots extracted from a cluster's movie. Arrows in the image highlight structural fluctuations observed during movie recording. Furthermore, there was no exchange of kDNA molecules between the cluster and its surrounding medium, suggesting that the depletion energy that binds the individual kDNA molecules together within a cluster is strong enough (a few k_BT) to maintain their collective integrity, yet flexible enough to allow for observed fluctuations in cluster morphology.

It's important to elucidate the notion of topology.[72] Herein, topology refers to the structure of a manifold, shaped by the inability of polymers to cross themselves. In the case of catenane, rings within the molecular network are unable to pass through one another or change their relative spatial positions because they are permanently interlocked. This interlocking is quantified by the average catenation valency of the rings for 2D and 3D catenated networks.[35,44] While the statistical properties of a single molecule of catenanes are well explored,[73–78] studies on catenane-linear blends are scarce.[43,79] To the best of our knowledge, this is the first experimental study presenting the bulk phase behavior of a topologically complex DNA network, resembling a 2D Olympic gel polymer, in the presence of linear DNA.

4. Conclusions and outlook

In conclusion, our study examines the critical role of topology in dictating the phase behavior of polymeric blends. Specifically, we studied the phase behavior of the 2D catenated network of DNA rings, known as kinetoplasts, in the presence of linear DNA. While prior work shows that mixtures of circular and linear DNA always remain in the isotropic phase with enhanced miscibility, here we discovered that the assembly of catenated DNA rings results in phase separation in the presence of linear DNA. This distinction highlights how the topology of polymer components profoundly influences phase behavior in polymer blends. Furthermore, our investigation reveals that the phase-separated aggregates of kinetoplasts exhibit fractal characteristics, suggesting the dominance of a diffusion-limited mechanism in the aggregation process. The size of the individual cluster is very robust and presents hierarchical relaxation. Moreover, a key insight emerging from both previous studies[43] and the present work is that the equilibrium states of catenated-linear polymer blends are determined not only by their topological states, but are also highly sensitive to the ratio of catenane mesh size to polymer size. In the presence of 10 kDa PEG, kDNA undergoes intramolecular compaction, whereas λ-DNA induces only intermolecular aggregation without disrupting the internal structure of individual kDNA networks. While these contrasting behaviors are primarily attributed to differences in linear polymer size relative to the kDNA mesh, other factors, such as bending rigidity (persistence length) and the chemical nature of the linear polymers may likely influence their interactions with the kDNA network. A deeper understanding of these effects could be achieved through systematic studies varying the size of PEG and DNA depletants. Additionally, exploring the ionic strength dependence of phase behavior may further clarify the role of electrostatic interactions in governing kDNA assembly.

Recent advances in the synthesis of both covalent 2D polymers[80] and Olympic gels of varying spatial dimension and catenation valency[33,81,82] highlight the need to understand their phase behavior, particularly when combined with other polymer structures. In addition to materials science, topological features play a crucial role in biological systems. For example, in the presence of macromolecular crowders, the phase behavior of DNA is highly sensitive to its topological state.[83,84] Supercoiling, for example, facilitates the compaction of plasmids and is a key factor in controlling chromosome compaction within the nucleus.[20,85] By exploring the influence of catenation valency[44,48] and the relaxed *versus* supercoiled state of individual rings within the catenated network, we can map a wide spectrum of phase behavior in parameter space. This type of study will not only guide us in designing new complex materials but also enhance our understanding of

chromosome packing in different species, particularly in kinetoplastida where diverse topological states of DNA are observed.[86] We envision our research as a catalyst for deeper exploration of the phase behavior of 2D topological soft matter when combined with polymers of diverse architectures, thereby fostering advancements in the design and development of novel polymeric materials with tailored properties.

Conflicts of interest

There are no conflicts to declare.

Data availability

The data supporting the findings of this study are presented in the manuscript and the SI. Calculation of excluded volume of kDNA and effective overlap concentration of λ-DNA. Scaling arguments of imaging times, autocorrelation and cross-correlation analyses of structural fluctuations. Figures show temporal evolution of kDNA aggregates at varying λ-DNA concentration, schematic illustrating the size-dependent penetration of polymers into kDNA mesh, cross-correlation plots, and time laps movies (10X speed) capturing the thermal fluctuations of kDNA aggregates. See DOI: **https://doi.org/10.1039/d5sm00461f**

Acknowledgements

This project was funded by NSF Grant CBET-1936696. We thank Dr. Cassandra Rogers of the W. M. Keck Facility for Biological Imaging at the Whitehead Institute for her support in confocal imaging. We acknowledge partial support from the National Science Foundation grant CBET-2510937 to PSD.

References

1 W. M. Jacobs and D. Frenkel, Phase transitions in biological systems with many components, *Biophys. J.*, 2017, **112**, 683.
2 M. Dijkstra, R. van Roij and R. Evans, Phase behavior and structure of binary hard-sphere mixtures, *Phys. Rev. Lett.*, 1998, **81**, 2268.
3 H. N. Lekkerkerker, W.-K. Poon, P. N. Pusey, A. Stroobants and P. Warren, Phase behaviour of colloid+ polymer mixtures, *Europhys. Lett.*, 1992, **20**, 559.
4 S. Assenza and R. Mezzenga, Soft condensed matter physics of foods and macronutrients, *Nat. Rev. Phys.*, 2019, **1**, 551.
5 A. Christensen, A. V. Ruban, P. Stoltze, K. W. Jacobsen, H. L. Skriver, J. K. Nørskov and F. Besenbacher, Phase diagrams for surface alloys, *Phys. Rev. B: Condens. Matter Mater. Phys.*, 1997, **56**, 5822.
6 M. W. Matsen, Effect of architecture on the phase behavior of ab-type block copolymer melts, *Macromolecules*, 2012, **45**, 2161.
7 A. Milchev, S. A. Egorov, J. Midya, K. Binder and A. Nikoubashman, Entropic unmixing in nematic blends of semiflexible polymers, *ACS Macro Lett.*, 2020, **9**, 1779.
8 M. E. Helgeson, S. E. Moran, H. Z. An and P. S. Doyle, Mesoporous organohydrogels from thermogelling photocrosslinkable nanoemulsions, *Nat. Mater.*, 2012, **11**, 344.
9 A. Scacchi, S. J. Nikkhah, M. Sammalkorpi and T. Ala-Nissila, Self-assembly in soft matter with multiple length scales, *Phys. Rev. Res.*, 2021, **3**, L022008.
10 F. S. Bates, Polymer-polymer phase behavior, *Science*, 1991, **251**, 898.
11 K. Zhao and T. G. Mason, Assembly of colloidal particles in solution, *Rep. Prog. Phys.*, 2018, **81**, 126601.
12 C. Zhang, P. G. Shao, J. A. van Kan and J. R. van der Maarel, Macromolecular crowding induced elongation and compaction of single dna molecules confined in a nanochannel, *Proc. Natl. Acad. Sci. U. S. A.*, 2009, **106**, 16651.
13 C. P. Brangwynne, C. R. Eckmann, D. S. Courson, A. Rybarska, C. Hoege, J. Gharakhani, F. Julicher and A. A. Hyman, Germline p granules are liquid droplets that localize by controlled dissolution/condensation, *Science*, 2009, **324**, 1729.
14 Y. Shin and C. P. Brangwynne, Liquid phase condensation in cell physiology and disease, *Science*, 2017, **357**, eaaf4382.
15 T. C. Michaels, D. Qian, A. Saric, M. Vendruscolo, S. Linse and T. P. Knowles, Amyloid formation as a protein phase transition, *Nat. Rev. Phys.*, 2023, **5**, 379.
16 A. J. DeStefano, R. A. Segalman and E. C. Davidson, Where biology and traditional polymers meet: The potential of associating sequence-defined polymers for materials science, *JACS Au*, 2021, **1**, 1556.
17 S. Chu, Biology and polymer physics at the single–molecule level, *Philos. Trans. R. Soc., A*, 2003, **361**, 689.
18 C. P. Brangwynne, P. Tompa and R. V. Pappu, Polymer physics of intracellular phase transitions, *Nat. Phys.*, 2015, **11**, 899.
19 M. T. van Loenhout, M. De Grunt and C. Dekker, Dynamics of dna supercoils, *Science*, 2012, **338**, 94.
20 J. D. Halverson, J. Smrek, K. Kremer and A. Y. Grosberg, From a melt of rings to chromosome territories: the role of topological constraints in genome folding, *Rep. Prog. Phys.*, 2014, **77**, 022601.
21 A. R. Klotz, B. W. Soh and P. S. Doyle, Motion of knots in dna stretched by elongational fields, *Phys. Rev. Lett.*, 2018, **120**, 188003.
22 B. W. Soh, A. R. Klotz, R. M. Robertson-Anderson and P. S. Doyle, Long-lived self-entanglements in ring polymers, *Phys. Rev. Lett.*, 2019, **123**, 048002.
23 K. R. Peddireddy, M. Lee, C. M. Schroeder and R. M. Robertson-Anderson, Viscoelastic properties of ring-linear dna blends exhibit nonmonotonic dependence on blend composition, *Phys. Rev. Res.*, 2020, **2**, 023213.
24 Y. Zhou, K.-W. Hsiao, K. E. Regan, D. Kong, G. B. McKenna, R. M. Robertson-Anderson and C. M. Schroeder, Effect of molecular architecture on ring polymer dynamics in semidilute linear polymer solutions, *Nat. Commun.*, 2019, **10**, 1753.
25 D. Parisi, J. Ahn, T. Chang, D. Vlassopoulos and M. Rubinstein, Stress relaxation in symmetric ring-linear polymer blends at low ring fractions, *Macromolecules*, 2020, **53**, 1685.

26 D. G. Tsalikis and V. G. Mavrantzas, Size and diffusivity of polymer rings in linear polymer matrices: The key role of threading events, *Macromolecules*, 2020, **53**, 803.
27 M. Kruteva, J. Allgaier and D. Richter, Direct observation of two distinct diffusive modes for polymer rings in linear polymer matrices by pulsed field gradient (pfg) nmr, *Macromolecules*, 2017, **50**, 9482.
28 G. S. Grest, T. Ge, S. J. Plimpton, M. Rubinstein and T. C. O'Connor, Entropic mixing of ring/linear polymer blends, *ACS Polym. Au*, 2022, **3**, 209.
29 R. M. Robertson, S. Laib and D. E. Smith, Diffusion of isolated dna molecules: Dependence on length and topology, *Proc. Natl. Acad. Sci. U. S. A.*, 2006, **103**, 7310.
30 J. D. Halverson, G. S. Grest, A. Y. Grosberg and K. Kremer, Rheology of ring polymer melts: From linear contaminants to ring-linear blends, *Phys. Rev. Lett.*, 2012, **108**, 038301.
31 T. T. Perkins, S. R. Quake, D. E. Smith and S. Chu, Relaxation of a single dna molecule observed by optical microscopy, *Science*, 1994, **264**, 822.
32 M. Seiler, Hyperbranched polymers: Phase behavior and new applications in the field of chemical engineering, *Fluid Phase Equilib.*, 2006, **241**, 155.
33 L. F. Hart, J. E. Hertzog, P. M. Rauscher, B. W. Rawe, M. M. Tranquilli and S. J. Rowan, Material properties and applications of mechanically interlocked polymers, *Nat. Rev. Mater.*, 2021, **6**, 508.
34 J. Chen, C. A. Rauch, J. H. White, P. T. Englund and N. R. Cozzarelli, The topology of the kinetoplast DNA network, *Cell*, 1995, **80**, 61.
35 J. Chen, P. T. Englund and N. R. Cozzarelli, Changes in network topology during the replication of kinetoplast dna, *EMBO J.*, 1995, **14**, 6339.
36 D. Michieletto, D. Marenduzzo and E. Orlandini, Is the kinetoplast DNA a percolating network of linked rings at its critical point?, *Phys. Biol.*, 2015, **12**, 036001.
37 L. Ibrahim, P. Liu, M. Klingbeil, Y. Diao and J. Arsuaga, Estimating properties of kinetoplast DNA by fragmentation reactions, *J. Phys. A: Math. Theor.*, 2019, **52**, 034001.
38 T. A. Shapiro, Kinetoplast DNA maxicircles: Networks within networks, *Proc. Natl. Acad. Sci. U. S. A.*, 1993, **90**, 7809.
39 A. R. Klotz, B. W. Soh and P. S. Doyle, Equilibrium structure and deformation response of 2D kinetoplast sheets, *Proc. Natl. Acad. Sci. U. S. A.*, 2020, **117**, 121.
40 B. W. Soh and P. S. Doyle, Deformation Response of Catenated DNA Networks in a Planar Elongational Field, *ACS Macro Lett.*, 2020, **9**, 944.
41 B. W. Soh, A. Khorshid, D. Al Sulaiman and P. S. Doyle, Ionic Effects on the Equilibrium Conformation of Catenated DNA Networks, *Macromolecules*, 2020, **53**, 8502.
42 B. W. Soh and P. S. Doyle, Equilibrium Conformation of Catenated DNA Networks in Slitlike Confinement, *ACS Macro Lett.*, 2021, **10**, 880–885.
43 I. Yadav, D. Al Sulaiman, B. W. Soh and P. S. Doyle, Phase Transition of Catenated DNA Networks in Poly(ethylene glycol) Solutions, *ACS Macro Lett.*, 2021, **10**, 1429.
44 I. Yadav, D. Al Sulaiman and P. S. Doyle, Tuning the topology of a two-dimensional catenated dna network, *Phys. Rev. Res.*, 2023, **5**, 013141.
45 J. Ragotskie, N. Morrison, C. Stackhouse, R. C. Blair and A. R. Klotz, The effect of the kinetoplast edge loop on network percolation, *J. Polym. Sci.*, 2024, **62**, 1287–1295.
46 P. He, A. J. Katan, L. Tubiana, C. Dekker and D. Michieletto, Single-molecule structure and topology of kinetoplast dna networks, *Phys. Rev. X*, 2023, **13**, 021010.
47 D. P. Cavalcanti, D. L. Goncalves, L. T. Costa and W. de Souza, The structure of the kinetoplast DNA network of Crithidia fasciculata revealed by atomic force microscopy, *Micron*, 2011, **42**, 553.
48 S. Ramakrishnan, Z. Chen, Y. A. G. Fosado, L. Tubiana, W. Vanderlinden, N. J. Savill, A. Schnaufer and D. Michieletto, Single-molecule morphology of topologically digested olympic networks, PRX, *Life*, 2024, **2**, 013009.
49 B. Diggines, S. Whittle, I. Yadav, E. P. Holmes, D. E. Rollins, T. E. Catley, P. S. Doyle and A. L. Pyne, Multiscale topological analysis of kinetoplast dna via highresolution afm, *Phys. Chem. Chem. Phys.*, 2024, **26**, 25798.
50 A. Balducci, P. Mao, J. Han and P. S. Doyle, Doublestranded dna diffusion in slitlike nanochannels, *Macromolecules*, 2006, **39**, 6273.
51 S. Banik, D. Kong, M. J. San Francisco and G. B. McKenna, Monodisperse lambda dna as a model to conventional polymers: A concentration-dependent scaling of the rheological properties, *Macromolecules*, 2021, **54**, 8632.
52 P. Khanal, K. R. Peddireddy, J. Marfai, R. McGorty and R. M. Robertson-Anderson, Dna topology dictates emergent bulk elasticity and hindered macromolecular diffusion in dna-dextran composites, *J. Rheol.*, 2022, **66**, 699.
53 K. R. Peddireddy, D. Michieletto, G. Aguirre, J. Garamella, P. Khanal and R. M. Robertson-Anderson, Dna conformation dictates strength and flocculation in dna–microtubule composites, *ACS Macro Lett.*, 2021, **10**, 1540.
54 L. Onsager, The effects of shape on the interaction of colloidal particles, *Ann. N. Y. Acad. Sci.*, 1949, **51**, 627.
55 X. Zhu, B. Kundukad and J. R. van der Maarel, Vis11 coelasticity of entangled λ-phage dna solutions, *J. Chem. Phys.*, 2008, **129**, 185103.
56 Z. Gong and J. R. van der Maarel, Translational and reorientational dynamics of entangled dna, *Macromolecules*, 2014, **47**, 7230.
57 D. Asnaghi, M. Carpineti, M. Giglio and M. Sozzi, Coagulation kinetics and aggregate morphology in the intermediate regimes between diffusion-limited and reactionlimited cluster aggregation, *Phys. Rev. A: At., Mol., Opt. Phys.*, 1992, **45**, 1018.
58 L. Wu, C. P. Ortiz and D. J. Jerolmack, Aggregation of elongated colloids in water, *Langmuir*, 2017, **33**, 622.
59 D. A. Weitz and M. Oliveria, Fractal structures formed by kinetic aggregation of aqueous gold colloids, *Phys. Rev. Lett.*, 1984, **52**, 1433.
60 T. A. Witten and L. M. Sander, Diffusion-limited aggregation, *Phys. Rev. B: Condens. Matter Mater. Phys.*, 1983, **27**, 5686.

61 H. Wu, M. Lattuada and M. Morbidelli, Dependence of fractal dimension of dlca clusters on size of primary particles, *Adv. Colloid Interface Sci.*, 2013, **195**, 41.
62 P. Meakin, Diffusion-controlled cluster formation in 2-6 dimensional space, *Phys. Rev. A: At., Mol., Opt. Phys.*, 1983, **27**, 1495.
63 S. Asakura and F. Oosawa, On interaction between two bodies immersed in a solution of macromolecules, *J. Chem. Phys.*, 1954, **22**, 1255.
64 N. Yaffe, D. Rotem, A. Soni, D. Porath and J. Shlomai, Direct monitoring of the stepwise condensation of kinetoplast DNA networks, *Sci. Rep.*, 2021, **11**, 1.
65 H. N. Lekkerkerker, R. Tuinier and M. Vis, *Colloids and the depletion interaction*, Springer Nature, 2024.
66 R. Verma, J. C. Crocker, T. C. Lubensky and A. Yodh, Attractions between hard colloidal spheres in semiflexible polymer solutions, *Macromolecules*, 2000, **33**, 177.
67 R. Verma, J. C. Crocker, T. C. Lubensky and A. G. Yodh, Entropic colloidal interactions in concentrated dna solutions, *Phys. Rev. Lett.*, 1998, **81**, 4004.
68 C. C. Hsieh, A. Balducci and P. S. Doyle, An experimental study of DNA rotational relaxation time in nanoslits, *Macromolecules*, 2007, **40**, 5196.
69 M. Doi and S. F. Edwards, *The Theory of Polymer Dynamics*, Oxford University Press, New York, 1988.
70 I. Yadav, W. Rosencrans, R. Basak, J. A. van Kan and J. R. C. van der Maarel, Intramolecular dynamics of dsDNA confined to a quasi-one-dimensional nanochannel, *Phys. Rev. Res.*, 2020, **2**, 013294.
71 T. A. Weber and E. Helfand, Time-correlation functions from computer simulations of polymers, *J. Phys. Chem.*, 1983, **87**, 2881.
72 L. Tubiana, G. P. Alexander, A. Barbensi, D. Buck, J. H. Cartwright, M. Chwastyk, M. Cieplak, I. Coluzza, S. Copar and D. J. Craik, *et al.*, Topology in soft and biological matter, *Phys. Rep.*, 2024, **1075**, 1.
73 Z. A. Dehaghani, I. Chubak, C. N. Likos and M. R. Ejtehadi, Effects of topological constraints on linked ring polymers in solvents of varying quality, *Soft Matter*, 2020, **16**, 3029.
74 P. M. Rauscher, S. J. Rowan and J. J. de Pablo, Topological effects in isolated poly [n] catenanes: Molecular dynamics simulations and rouse mode analysis, *ACS Macro Lett.*, 2018, **7**, 938.
75 J. M. Polson, E. J. Garcia and A. R. Klotz, Flatness and intrinsic curvature of linked-ring membranes, *Soft Matter*, 2021, **17**, 10505.
76 P. Chiarantoni and C. Micheletti, Linear catenanes in channel confinement, *Macromolecules*, 2023, **56**, 2736.
77 J. Luengo-Marquez, S. Assenza and C. Micheletti, Shape and size tunability of sheets of interlocked ring copolymers, *Soft Matter*, 2024, **20**, 6595.
78 A. R. Klotz, C. J. Anderson and M. S. Dimitriyev, Chirality effects in molecular chainmail, *Soft Matter*, 2024, **20**, 7044.
79 R. Stano, C. N. Likos and S. A. Egorov, Mixing linear polymers with rings and catenanes: Bulk and interfacial behavior, *Macromolecules*, 2023, **56**, 8168.
80 J. W. Colson and W. R. Dichtel, Rationally synthesized two-dimensional polymers, *Nat. Chem.*, 2013, **5**, 453.
81 J.-K. Sun, Q.-X. Yao, Z.-F. Ju and J. Zhang, 2d selfcatenated coordination polymer constructed by tripleand double-helical chains, *CrystEngComm*, 2010, **12**, 1709.
82 T. L. Schmidt and A. Heckel, Construction of a structurally defined double-stranded dna catenane, *Nano Lett.*, 2011, **11**, 1739.
83 A. N. Gupta and J. R. van der Maarel, Compaction of plasmid dna by macromolecular crowding, *Macromolecules*, 2017, **50**, 1666.
84 M. Joyeux, Bacterial nucleoid: interplay of dna demixing and supercoiling, *Biophys. J.*, 2020, **118**, 2141.
85 R. N. Irobalieva, J. M. Fogg, D. J. Catanese Jr, T. Sutthibutpong, M. Chen, A. K. Barker, S. J. Ludtke, S. A. Harris, M. F. Schmid and W. Chiu, *et al.*, Structural diversity of supercoiled dna, *Nat. Commun.*, 2015, **6**, 8440.
86 J. Lukes, D. Lys Guilbride, J. Votypka, A. Zıkova, R. Benne and P. T. Englund, Kinetoplast dna network:evolution of an improbable structure, *Eukaryotic Cell*, 2002, **1**, 495.